Vietnam Journal of Earth Sciences, 45(3), 287-302, https://doi.org/10.15625/2615-9783/18410

Vietnam Journal of Earth Sciences
https://vjs.ac.vn/index.php/jse

Contribution of advanced edge detection filters for the structural mapping of the Douala Sedimentary Basin along the Gulf of Guinea

Paul Gautier Kamto[1,2*], Erdinc Oksum[3], Luan Thanh Pham[4], Joseph Kamguia[1,2]

[1]*Research Laboratory in Geodesy, National Institute of Cartography (NIC), Yaounde, Cameroon*
[2]*Department of Physics, Faculty of Science, University of Yaounde I, Yaounde, Cameroon*
[3]*Department of Geophysical Engineering, Süleyman Demirel University, Isparta, Turkey*
[4]*Faculty of Physics, University of Science, Vietnam National University, Hanoi, Vietnam*

Received 15 March 2023; Received in revised form 22 May 2023; Accepted 8 June 2023

ABSTRACT

The Douala sedimentary basin (DSB) is an area of interest because of its hydrocarbon potential. Geophysical investigations in this basin are necessary to understand its structural features better. In this study, we aimed to highlight the major lineaments of the DSB by interpreting gravity data using advanced edge detection filters based on various combinations of the horizontal and vertical gradients of the field, namely the total horizontal gradient (THG), analytical signal (AS), theta map (TM), gradient amplitude of the vertical derivative (THG_VD), the tilt angle of the total horizontal gradient amplitude (TAHG) and a novel edge detector based on the soft sign function (SF). These filters were first tested on synthetic data of a simple density model to examine their effectiveness. The results show that the edges of the model structures can be visualized with greater accuracy using the TAHG and SF filters compared to the results from the others.

Further, although the TAHG and SF filters produced good results in identifying shallow and deep structures, solutions from SF proved to be better at delineating edges. Next, we applied these edge detection filters to the residual gravity anomaly of the study area obtained after a filtering process on the complete Bouguer anomaly. The SF filter clearly and accurately identifies the major structural features. The existence and location of previously unidentified lineaments have been shown. Most of the lineaments of the DSB extracted by this study provide geometric information on the lateral distribution of depositional successions filling the basin. The structural features are mainly concentrically from the volcanic center of Mount Cameroon and show that the DSB has probably been affected by earthquakes from the permanent activities of the Cameroon volcanic line since the Cretaceous. The highlighted lineaments of the DSB obtained from this study may shed light on future studies to improve mineral/hydrocarbon exploitation and update the area's geological/tectonic information.

Keywords: Gravity data, edge detection, lineaments, Douala Sedimentary Basin.

1. Introduction

The Douala Sedimentary Basin (DSB) is along the Gulf of Guinea. According to its structural characteristics, it belongs to the Aptian salt basin of equatorial west Africa (Brownfield and Charpentier, 2006). Fig. 1 presents the location of the study area, between the latitudes 3°30'N and 4°40'N and longitudes 9°10'N and 10°20'E. This basin

*Corresponding author, Email: gautier1994@yahoo.fr

extends under the waters of the Gulf of Guinea by a 25 km wide continental platform and covers a total surface area of 19,000 km^2 (Mbesse et al., 2012). The formation of the DSB resulted from the gradual North-South opening of the South Atlantic Ocean, causing the diachronism of deposits from south to north and a temporal and spatial variation of sedimentary environments along coastal West Africa (Kenfack et al., 2012). This basin's morphology and geological structure are related to some tectonic plate motions which have affected the sedimentary layer on the surface (Morley, 1995). The DSB is an area of interest because of its hydrocarbon potential. The potential field methods play an important role in structural mapping (Hinze et al., 2013; Elkhateeb and Abdellatif, 2018; Pham et al., 2019; Oksum et al., 2019; Kamto et al., 2021). Knowledge of the gravity field source edges is essential in exploring hydrocarbon resources. A high-precision structural map over the sedimentary basin could be used to update the geological map of the study area. Thus, a high-resolution edge detector filter is required to precisely delineate the boundaries of buried structures in this basin.

Gravity data are useful in determining the crustal lineament patterns in near-surface geophysics. The boundaries of geological structures are related to discontinuities or contacts between different formations. Various techniques based on derivatives of gravity data have been developed to outline the boundaries of subsurface structures (Cordell and Grauch, 1985; Roest et al., 1992; Hsu et al., 1996; Fedi and Florio, 2001; Bournas and Baker, 2001; Cella et al., 2009). However, the main disadvantage of these methods is that they cannot simultaneously highlight the edges of shallow and deep sources (Ma et al., 2014; Eldosouky et al., 2020; Pham et al., 2018; 2022; 2023). To resolve this problem, many phase-based edge detector filters that can produce balanced results have been developed (Wijns et al., 2005; Cooper and Cowan, 2006; Ferreira et al., 2013; Yuan and Yu, 2015). Although the phase-based methods can simultaneously equalize large and small amplitudes, they may outline unrealistic source edges. The boundaries of gravity sources are diffused, and the highlighted trends differ when the choice of size of the window is changed (Pham et al. 2021). Several authors have developed other filters to delineate the horizontal boundaries of deep and shallow sources (e.g., Zhang et al., 2015; Nasuti and Nasuti, 2018; Nasuti et al., 2019; Zareie and Moghadam, 2019). The main disadvantage of these filters is that the recognized boundaries of deep sources can appear more expansive than their actual size. Pham et al. (2021) proposed a new high-resolution filter based on the soft sign function and the derivatives of the horizontal gradient to outline the horizontal boundaries of geological structures with high precision.

In this paper, we aim to contribute to a better understanding of the structural configuration of the DSB by interpreting the gravity data within the scope of boundary analyses using advanced edge detection methods. We applied different edge detection filters, particularly the total horizontal gradient [THG] (Cordell and Grauch, 1985), which is a conventional detector commonly used for edge estimation, the analytical signal [AS] (Roest et al., 1992), the theta map (TM) introduced by Wijns et al. (2005) that normalizes the total gradient using the gradient amplitude to achieve balanced images from shallow and deep sources, the gradient amplitude of the vertical derivative [THG_VD] proposed by Tatchum et al. (2011), the tilt angle of the total horizontal gradient amplitude [TAHG] (Ferreira et al., 2013) and the edge detector filter based on the soft sign function (SF) introduced by Pham et al. (2021). The effectiveness of the methods has been estimated on a simple density model before the application on the natural field data of the study area. The study is organized into four sections. We briefly describe the

geological and tectonic settings of the study area in Section 2. The data and methods used are detailed in Section 3 and Section 4. Section 5 presents a synthetic data case demonstrating the effectiveness of the edge detector filters. Section 6 presents the results. Finally, the study is discussed and concluded in Section 7.

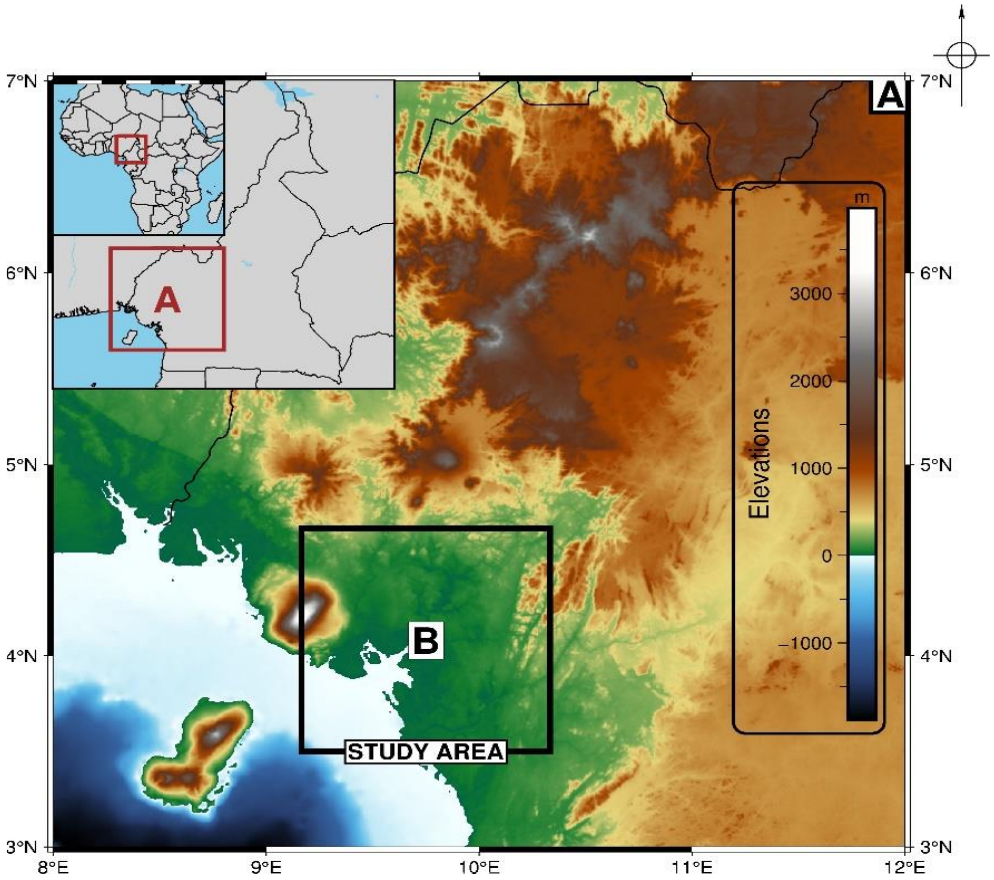

Figure 1. Location map of the study area. Topographic and bathymetric data are taken from the 1 arcminute global relief model ETOPO1 (Amante and Eakins, 2009)

2. Geological and tectonic settings

The DSB is part of the Equatorial Atlantic Margin rift system. The geological formations of the DSB resulted from the gradual North-South opening of the South Atlantic Ocean in the Early Cretaceous, causing the diachronism of deposits from south to north and a temporal and spatial variation of sedimentary environments along West Africa's coastal areas (Kenfack et al., 2012). The geology of the study area is dominated by an accumulation of sediments ranging from Cretaceous to Quaternary age overlying a Precambrian basement (Fig. 2). The DSB is covered by continental and marine deposits, especially mudstones, calcareous mudstones, arkosic sandstones, fine to coarse-grained sandstones, siltstones, sands, and dolomites. Mfayakouo et al. (2014) and Kwetche et al. (2018) assumed that some formations of the DSB started with fluvial continental deposits at the lowermost part and ended with coastal margin marine deposits in the upper part. Previous geological studies estimated the depth of the sedimentary section to be 8 to 10 km.

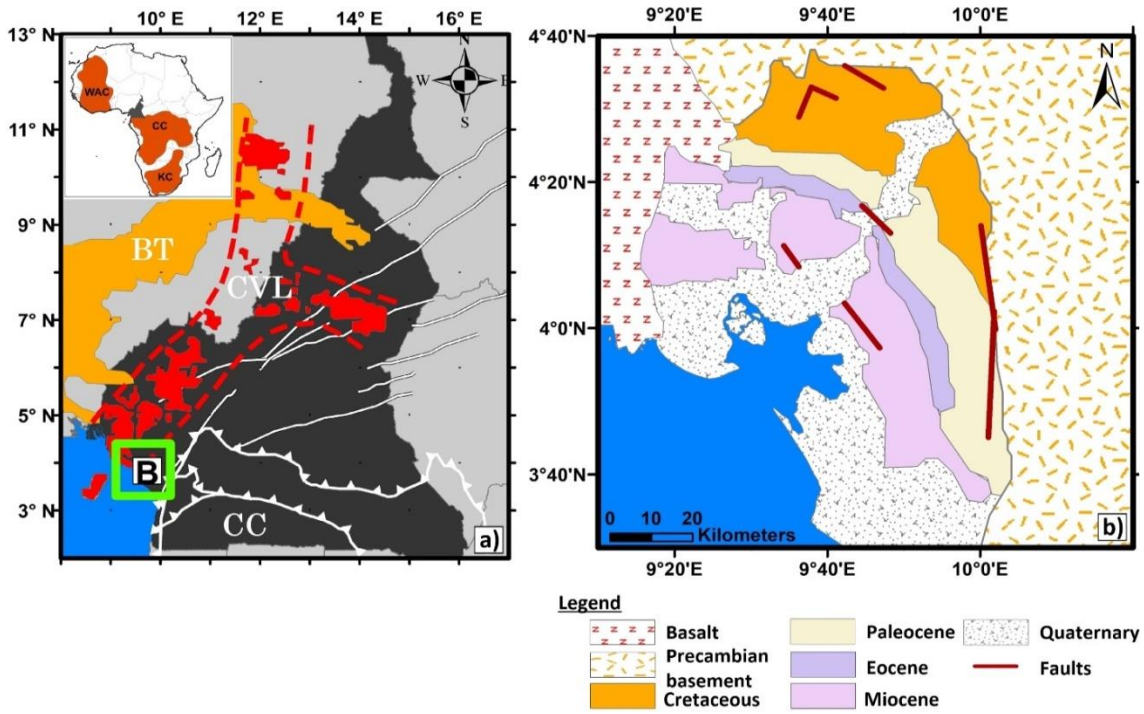

Figure 2. Geological map of the Douala sedimentary basin (after Pauken et al. 1991; Lawrence et al. 2002). The main geological units constituting the study area are represented on the dial b. The dial a) highlights the location of the study area in a region of the African plate. The major geological structures enhanced are: The Benue Through (BT), the Congo Craton (CC) and the Cameroon Volcanic Line (CVL)

Since the separation of Africa from South America during the Cretaceous period, three major tectonic events affected the DSB: an initial rifting phase in the early Cretaceous, a passive drift phase during the Late Cretaceous, and a short compressive episode in the Tertiary (Pauken et al., 1991; Meyers et al., 1996; Lawrence et al., 2002). During these phases, the DSB recorded some depositional sequences making about seven major Formations related to its evolution (Nguene et al., 1992; Brownfield and Charpentier, 2006). According to Kenfack et al. (2012), the development of the DSB was marked by: the deposition of Jurassic continental sediments, listric faulting during the Jurassic-Barremian; an intensive erosion activity of the highlands and deposition in the previously formed graben; salt deposition, and transform development resulting in a series of cross-faults that segmented the rift structure; and marginal clastic sedimentation.

The continental breakup of Pangea into the American and African plates during the Aptian-Albian was followed by the reactivation of discontinuities dating from the Pan-African orogeny (650 to 450 Ma). Some of these large reactivated structures constitute the Pernambouc-Tiko-Adamawa fracture system. This set of fractures was followed by the formation of Douala/Kribi-Campo basin (Nguene et al., 1992; Lawrence et al., 2002). Additionally, the continental fracturing led to the formation of listric faults at the depth that caused uneven sedimentation above the tilting of the blocks during the general stretching.

3. Data

Gravity data are widely used to highlight geological and tectonic structures, both deep

and shallow. Due to their high-resolution, satellite gravity models have recently shown great success in the detection of gravity field sources and the boundary identification of geological structures (Pal et al., 2017; Kumar et al., 2020; Chouhan, 2020; Pham et al., 2021). This study uses the high-resolution gravity field model XGM2019e (Zingerle et al., 2020). This model was developed by combining many data sources (satellite gravity data from GOCO06s model, ground gravity data, and satellite altimetry model). The satellite model GOCO06s covered the long wavelengths up to degree and order (d/o) 300. The spherical harmonics coefficients of XGM2019e range up to d/o 5399 and the spatial resolution of this model is evaluated to approximately 2′ (~4 km). Free-air gravity anomalies have been derived from this gravity model and computed on ICGEM website with a spatial resolution of 1 arcminute.

We applied Bouguer corrections to the Free-air gravity anomalies to obtain complete Bouguer anomalies (Fig. 3) of the DSB from the XGM2019e model. An average density of 2.67 g/cm^3 has been assumed during the computation of topographic corrections, including the Bouguer plate and terrain correction. The 1 arcminute global relief model ETOPO1 (Amante and Eakins, 2009) was used to provide the study area's topographic and ocean bathymetry data. The Bouguer anomaly map shows amplitudes ranging from -47 mGal to 177 mGal. The maximum amplitude observed coincides with the location of Mount Cameroon, a major geological structure that limits the DSB in its northwestern part.

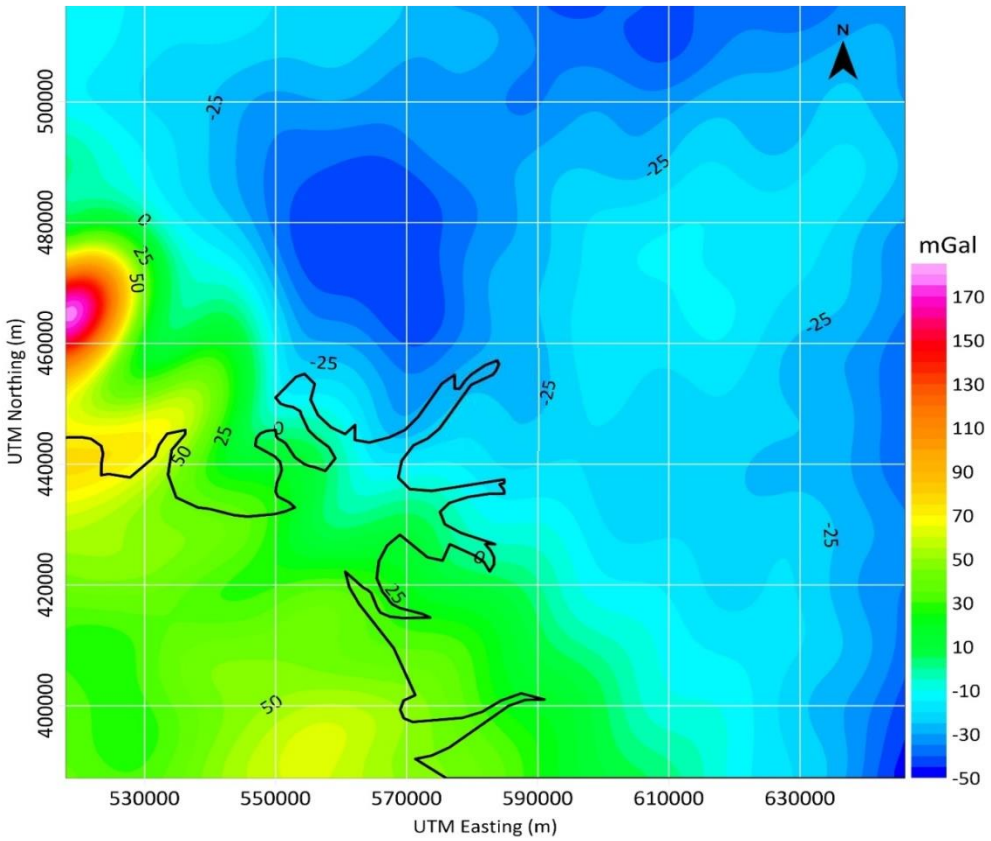

Figure 3. Complete Bouguer anomaly map of the DSB and its surroundings (Contour interval in 5 mGal)

4. Methods

Before describing the method employed for edge detection, we present an abridged description of filtering techniques used in the identification of buried bodies. The total horizontal gradient is one of the most popular methods for enhancing the edges of gravity data. The total horizontal gradient (THG) of the field F is defined by (Cordell and Grauch, 1985):

$$\mathrm{THG} = \sqrt{\left(\frac{\partial \mathrm{F}}{\partial \mathrm{x}}\right)^2 + \left(\frac{\partial \mathrm{F}}{\partial \mathrm{y}}\right)^2}. \quad (1)$$

The analytical signal is another popular filter for detecting the edges of geological structures, which is expressed (Roest et al., 1992):

$$\mathrm{AS} = \sqrt{\left(\frac{\partial \mathrm{F}}{\partial \mathrm{x}}\right)^2 + \left(\frac{\partial \mathrm{F}}{\partial \mathrm{y}}\right)^2 + \left(\frac{\partial \mathrm{F}}{\partial \mathrm{z}}\right)^2}. \quad (2)$$

Wijns et al. (2005) introduced the theta map method to provide balanced images for the edges. The equation of this method can be shown as follows:

$$TM = acos \frac{\sqrt{\left(\frac{\partial F}{\partial x}\right)^2 + \left(\frac{\partial F}{\partial y}\right)^2}}{\sqrt{\left(\frac{\partial F}{\partial x}\right)^2 + \left(\frac{\partial F}{\partial y}\right)^2 + \left(\frac{\partial F}{\partial z}\right)^2}}. \quad (3)$$

Tatchum et al. (2011) introduced an enhanced version of the total horizontal gradient that uses the high-order derivatives of gravity data to improve the resolution of the results. The filter is calculated as the following equation:

$$THG\_VD = \sqrt{\left(\frac{\partial VD}{\partial x}\right)^2 + \left(\frac{\partial VD}{\partial y}\right)^2}. \quad (4)$$

Where VD is the vertical gradient of the field.

Ferreira et al. (2013) calculated the tilt angle of the total horizontal gradient to detect the edge. The method is formulated as:

$$\mathrm{TAHG} = \mathrm{atan} \frac{\frac{\partial \mathrm{THG}}{\partial \mathrm{z}}}{\sqrt{\left(\frac{\partial \mathrm{THG}}{\partial \mathrm{x}}\right)^2 + \left(\frac{\partial \mathrm{THG}}{\partial \mathrm{y}}\right)^2}}. \quad (5)$$

Recently, Pham et al. (2021) suggested using the soft sign function filter that is based on the derivatives of the horizontal gradient of the potential field data. The soft sign function is calculated using the following equation:

$$\mathrm{SF} = \frac{\mathrm{k} \times \mathrm{THG_z} - (\mathrm{k}+2)\sqrt{(T\mathrm{HG_x})^2 + \left(T\mathrm{HG_y}\right)^2}}{\sqrt{(T\mathrm{HG_x})^2 + \left(\mathrm{THG_y}\right)^2} + \left|\mathrm{k} \times \mathrm{THG_z} - (\mathrm{k}+1)\sqrt{(\mathrm{THG_x})^2 + \left(T\mathrm{HG_y}\right)^2}\right|}, \quad (6)$$

where $\mathrm{THG_x}$, $\mathrm{THG_y}$ and $\mathrm{THG_z}$ are the x, y and z gradients of the horizontal gradient THG of the potential field data F, and k is an arbitrary positive real number. Values for k in the $1 \leq k \leq 10$ range yield the best results (Pham et al., 2021).

5. Synthetic Data Test

In this section, edge detection techniques used in this study are tested on synthetic data before applying them to real data, and their effectiveness in detecting edges is examined. Here we consider a simple gravity model that includes three superimposed prismatic source bodies (A, B, and C) at different depths and a slender source (D) placed next to them (Fig. 4a). The geometric parameters and the density contrasts of the model sources are given in Table 1. The synthetic gravity data produced by the model was calculated using the formulation by Rao et al. (1990) on a 201×201 grid with a square grid interval of

1 km. Fig. 4b illustrates the gravity anomaly map generated by the model. Fig. 5a displays the THG of the anomaly data in Fig. 4b. It can be seen in this figure that the THG method can distinguish the edges of the large C structure well, it detects the edges of the thin structure D. It cannot clearly detect the edges of the superimposed A and B structures on structure C. This is because the method cannot simultaneously separate the amplitude of structures at different depths or densities into components.

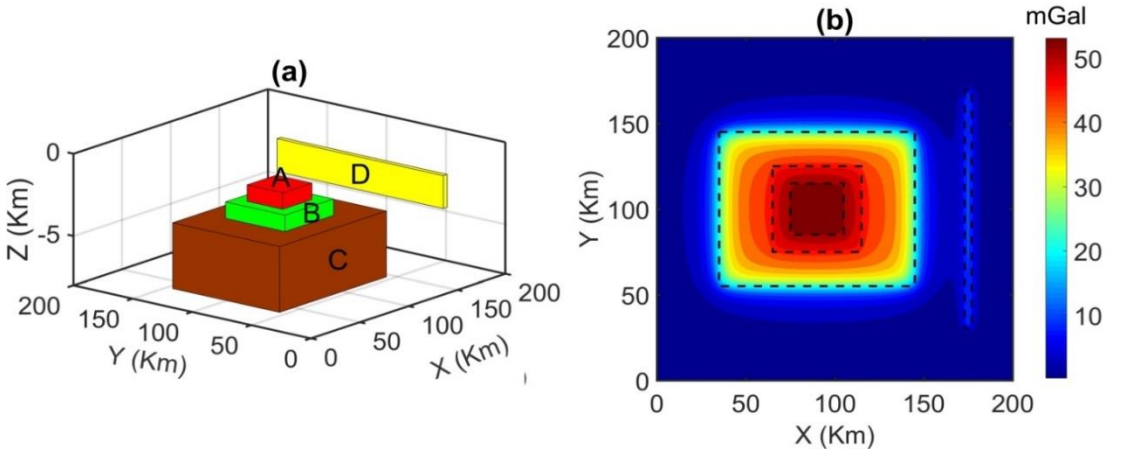

Figure 4. (a) Synthetic model with parameters given in Table 1, (b) synthetic gravity data of the model

Table 1. Parameters of the synthetic model

Parameters/Sources	A	B	C	D
x-coordinates of center (km)	90	90	90	175
y-coordinates of center (km)	100	100	100	100
Length (km)	30	50	110	140
Width (km)	30	50	90	4
Top depth (km)	2	3	4	2
Bottom depth (km)	3	4	8	4
Density contrast (g/cm^3)	0.1	0.2	0.3	0.3

Fig. 5b and 5c display the THG_VD and AS of the synthetic model in Fig. 4b, respectively. Although the THG_VD technique produced sharper responses over the thin and shallow source D, the obtained images for sources A, B, and C are fairly faint. If Fig.5a and Fig.5b are compared, the THG_VD is more effective in detecting edges of shallow sources. The AS filter can also detect the edges of the wide body C, but it cannot outline the edges of the thin source D, and as well it fails to draw the boundaries of A and B bodies due to not being effective in equalizing the amplitudes of different anomalies. Fig. 5d shows the edge detection results from the TM filter, where the minimum values give the location of the lateral boundaries.

Here, the TM filter produces results similar to the THG filter, but the response for the superimposed bodies A and B over body C appears more prominent. Although the TM method allows a more effective detection of the source boundaries compared with the THG, THG_VD and AS methods, as the depth increases, it is seen that the boundaries are obtained outside the real structure, thus making the structure appear more expansive than it is. Fig. 5e and 5f show the results determined by applying the TAHG and SF filters to the gravity anomaly of the synthetic model in Fig 4b, respectively. Both methods effectively balance the signal response from shallow and deep sources because all the boundaries of the A, B, C, and D structures that make up the model can be determined.

The use of these methods can also avoid producing some false boundaries. However, it is noteworthy that the SF shows peaks sharper over the edges compared to the TAHG. By comparing the results, we can see that the SF filter can not only delineate the edges of the sources more clearly and accurately but also give the high resolution of the edges.

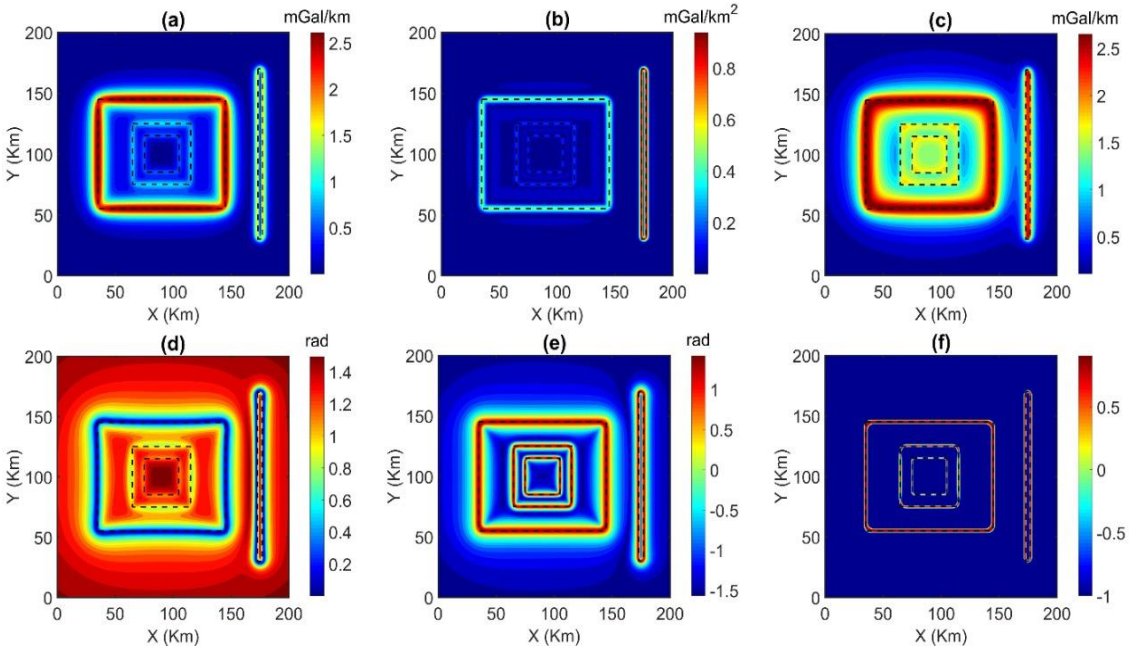

Figure 5. Edge detection results of filters applied on synthetic data (a) THG, (b) THG_VD, (c) AS, (d) TM, (e) TAHG, (f) SF

6. Results

6.1. Regional-residual separation and determination of the average depths

We shall concentrate now on the gravimetry of the DSB and variations around this geological structure. Still, before anything else, it is essential to mention that Bouguer gravity anomalies contain information on the gravitational contribution from several sources at different depths. In general, low-frequency components represent deep sources; high-frequency components are external noise sources. It is important to attenuate the gravity signal caused by deep sources to characterize shallow crustal structures better. Here, we used the radial average power spectrum (RAPS) of the Bouguer gravity anomaly to isolate anomalies of interest (residual gravity data) and to estimate the average depths to the density interfaces. The main advantage of the RAPS is that it does not require an assumption about the density contrast between bodies. To obtain the depths of the buried structures in the DSB, first, we transformed the Bouguer gravity anomaly into the frequency domain. A plot of the logarithm of the spectrum versus wavenumber is displayed in Fig. 6.

Then, we computed the average depths to the density interfaces directly from the slope of the logarithmic power spectral density as a function of the wavenumber. We observed that the first linear segment reveals the Conrad discontinuity at an average depth of 15 km. The second segment reveals other sources located at average depths of 10 km

representing the shallowest anomalous sources. The regional anomaly due to the Conrad structure was estimated by applying a low-pass filter using a cut-off wavenumber 0.025 km^{-1} (the intercept between the red and blue lines in Fig. 6). Finally, the residual gravity data generated by shallow density structures was computed by removing the regional anomaly from the Bouguer gravity data. Fig. 7 depicts the residual anomalies. The residual anomalies range between -39 and 143 mGal over the study area.

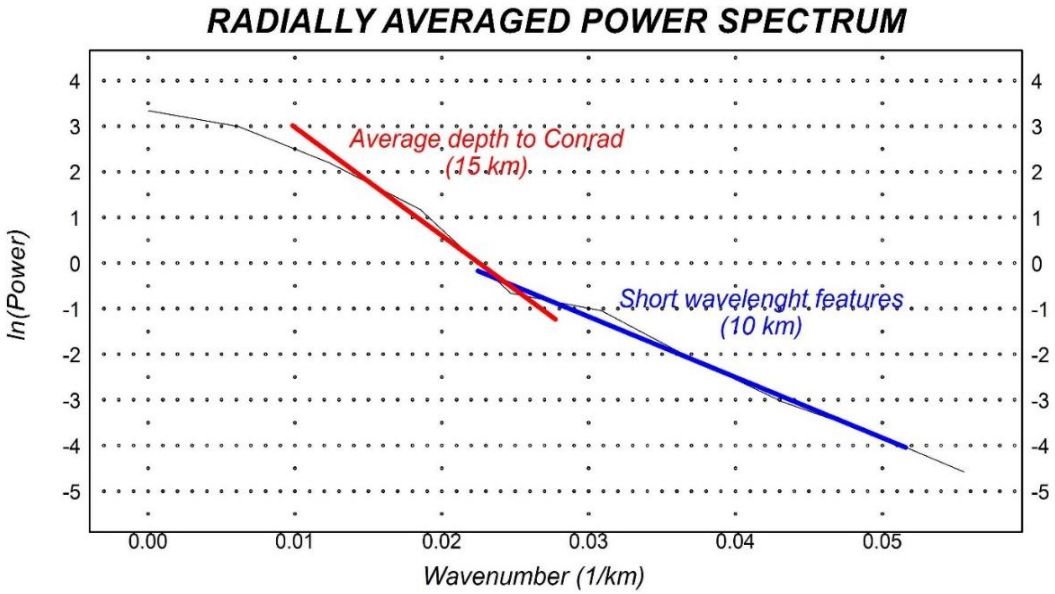

Figure 6. Radial average power spectrum of the Bouguer gravity anomaly

6.2. Edge enhancement of geological formations

We applied the edge detection filters to the residual gravity anomaly shown in Fig. 7 to determine abrupt lateral density variations in the DSB. These variations can be interpreted as subsurface structural discontinuities such as geological contacts or lateral changes in lithology. We compare the performance of the tested methods to delineate the location of geological edges in the DSB.

Fig. 8a shows the geological boundaries outlined by using the THG filter. By looking at Fig. 8a, we can say that the THG filter cannot define geological features satisfactorily. It seems that the edges of deep geological formations are not clearly highlighted. Fig. 8b shows the boundaries obtained from applying THG_VD filter. The THG_VD filter shows sharper features than those obtained with the THG filter. However, the limitations of the THG_VD filter are obvious as it makes contacts between adjacent amplitudes, thus causing the non-existent edges. We observe several other geological contacts not enhanced by the THG method. Fig. 8c displays the result determined from the application of the AS filter. The result obtained by the AS filter seems not to be satisfactory. Indeed, the edges of the highlighted geological formations are seen mostly blurred over the area whereas only the anomalies corresponding to Mount Cameroon's major geological structure appear distinctive.

Contrary to the results obtained by the two previous filters, the AS filter seems not to be effective in balancing the amplitudes of deep and shallow signatures. Fig. 8d shows the results obtained from applying the TM filter. Although the TM filter is suitable for equalizing signals from both shallow and deep sources, it introduces fictitious boundaries in the geological formations, thus making structural interpretation difficult. Fig. 8e depicts the result determined by applying the TAHG method. As for the TM filter, the TAHG filter is very effective in balancing the signal of geological boundaries, but the contacts created between these signals come to blur the real edges of the geological structures of the DSB. Fig. 8f shows the result obtained from the application of the SF filter. Despite the complex lithology of the study area, the SF filter can clearly and accurately identify the major geological boundaries. This filter also effectively highlights deep and shallow geological boundaries in the area.

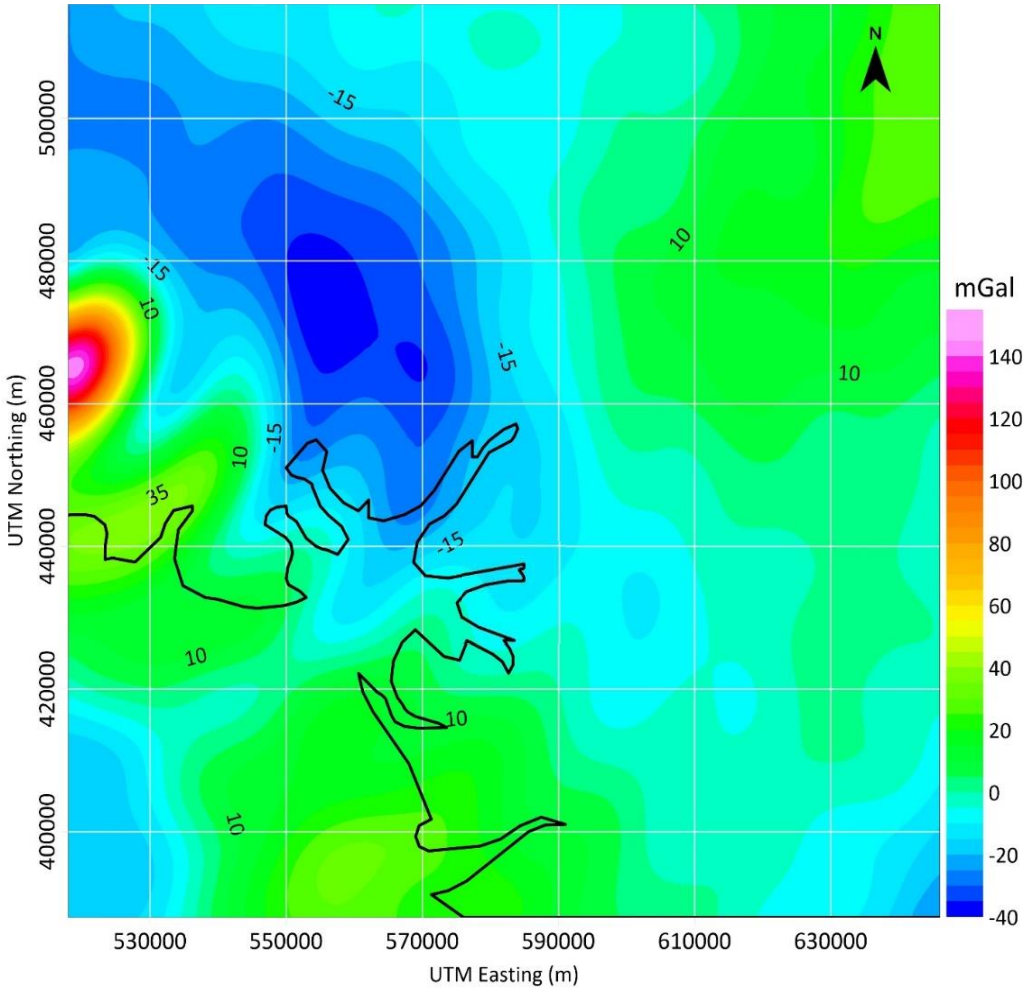

Figure 7. Residual Bouguer anomaly map of the study area used for the application of the edge detection filters (Contour interval in 5 mGal)

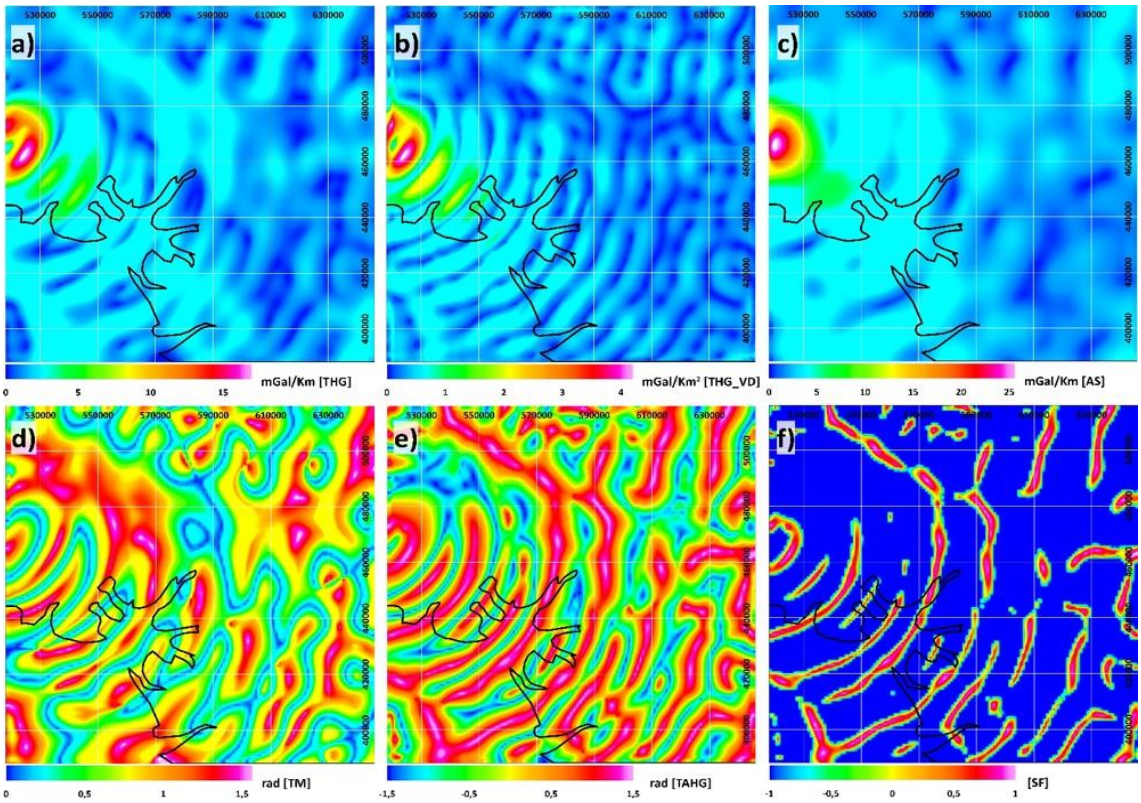

Figure 8. Application of edge filters to the residual gravity data from the Douala sedimentary basin. (a) THG, (b) THG_VD, (c) AS, (d) TM, (e) TAHG, (f) SF with k=3

7. Discussions

The study area is local and relatively small; identifying the lineaments in the DSB can show great limitations for the filters used. As indicated by their authors (Cordell and Grauch, 1985; Roest et al., 1992; Tatchum et al., 2011; Ferreira et al., 2013; Pham et al., 2021), the THG, THG_VD, AS, TAHG and SF methods maximize the signal amplitude over potential geological discontinuities in the study area; on the other hand, the TM filter (Wijns et al., 2005) reduces the signal amplitude to zero on the structural features of the basin. Despite the similarities observed in the results of the applied filters, significant differences can also be noted. Compared to the structures identified by the SF method, the THG, THG_VD, and AS methods show major limitations in identifying low amplitude features in the DSB. In addition, the high amplitude located on Mount Cameroon seems to induce false signals in the results produced by the THG_VD filter. By conducting a comparative analysis of a series of edge detection techniques, Eldosouky et al. (2020) and Pham et al. (2021) also showed that the THG and AS methods could have great difficulties in producing precise and high-resolution results on true geological contacts. The results displayed by the TM method are limited by their successive connection and false environmental signals. Several authors in the scientific literature have shown the poor performance of this filter, mainly due to the amplification of false structural features in the target area (Ting-Jie et al., 2016; Nasuti et al.,

2019; Eldosouky et al ., 2020; Oksum et al., 2021). Since the THG_VD, TAHG, and SF are based on second-order derivatives, they are more noise-sensitive than the conventional filters. However, this problem can be solved by the upward continuation of data before applying the filters, as shown by Ghomsi et al. (2022) and Eldosouky et al. (2022). Notably, the noise level in the Bouguer anomaly and residual data of the DSB is low. Therefore, applying the upward continuation filter to these datasets is unnecessary. Here, the best performances are observed for the TAHG and SF methods. However, compared to the TAHG filter, the SF filter performs better by minimizing any surrounding signal that can be attributed to a lineament. In other words, the SF filter can provide results with higher resolution than the TAHG filter and others. In addition, as shown in the model studies, the SF filter can avoid producing false information in the structural map.

Fig. 9 shows lineaments/geological contacts (light brown lines) extracted by the SF map with geological structures of the DSB. We found that the SF filter outperforms the other filters used in this study. It is worth noting that the result obtained from the SF filter clearly shows the directions and shapes of geological contacts/boundaries between sedimentary formations. The lineaments L1 and L2 marked on the map correspond to those previously identified by geological studies (Pauken et al., 1991; Lawrence et al., 2002). However, the SF filter could bring better precision to the location of these structural features. The other lineaments (dark brown lines) do not overlap with the features highlighted by the SF filter; therefore, additional studies should be invested in these structural features' existence or actual location. Beyond the identified lineaments, several other lineaments have been highlighted, thus showing the precision and sensitivity of the SF filter in enhancing geological discontinuity zones. Identifying these geological discontinuities both in the continental domain and the marine part is important for a region potentially rich in hydrocarbons. The concentric shapes observed probably reveal the direction of the evolution of shallow lithological formations. These results provide geometric information on the lateral distribution of the depositional series previously described by Nguene et al. (1992). New and previously unidentified structural features are highlighted.

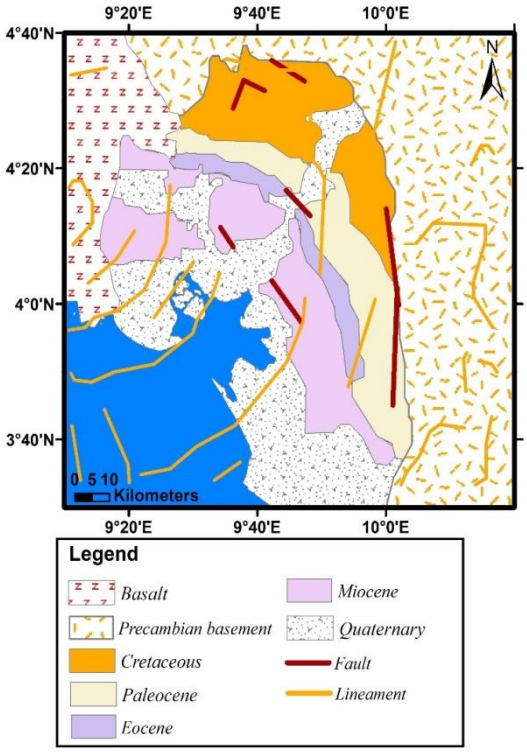

Figure 9. Lineaments/geological contacts (light brown lines) extracted from the SF map with geological structures. Geological map of the Douala sedimentary basin (after Pauken et al. 1991; Lawrence et al. 2002)

Furthermore, we note the absence of linear features due to the non-frustration of sedimentary rocks in this local region. Nguyen et al. (1992) announced that the formation of the DSB occurred after the

reactivation of large fractures in this region following the separation of the African and American lithospheric plates. The shape of these structural features has a great link with the paleoenvironmental evolution of the Douala sub-basin and could help for a better knowledge of the West African margin evolution. Furthermore, previous studies have not yet focused on the location of fractured zones within the Douala sub-basin. Van (2009) showed some deformed structures within the basin. Also, the results of Djomeni et al. (2011) showed the presence of deformed structures within the basin especially folded and brittle structures (faults, fractures, and joints). However, the location of the spatial extent of fractured zones has not been done. In addition, the latter showed that the study area's sedimentary rocks have probably been affected by earthquakes from the permanent activities of the Cameroon Volcanic Line (CVL) since the Cretaceous. Fig. 9 shows structural features evolving mainly concentrically from the volcanic center of Mount Cameroon. The highlighted structural features of the DSB are the main places for the migration of hydrocarbon resources. They could be used to improve mineral/hydrocarbon exploitation in this basin, and also to update geological/tectonic information in the area.

8. Conclusions

In this work, we applied various edge detection filters based on the combination of the horizontal and vertical gradients of the field, such as the THG, THG_VD, AS, TM, TAHG, and SF, to map the lineaments in the residual gravity anomaly data to better understand geological boundaries of the DSB along the Gulf of Guinea. Before applying those filters to actual gravity data from the study area, they were tested on synthetic data of a simple density model to examine their effectiveness in edge detection. The results demonstrate that the borders of the prismatic structures can be identified with great accuracy using the TAHG and SF filters. However, the solution of the SF proves to be sharper than the TAHG, though both of these filters can simultaneously equalize signals from shallow and deep structures. With this information, we used the filters on the gravity field data of the DSB. The SF filter identifies the study area's major geological contacts and lineaments. This recent edge detection method enables the identification of new lineaments in the sedimentary basin with unprecedented precision. It thus contributes to the knowledge of the structural geology of the study area. The geometric configuration of these lineaments clearly shows the lateral distribution of the geological (sedimentary) formations that make up the basin. The geological discontinuities take a concentric shape from the volcanic center of Mount Cameroon and indicate that the basin has probably been affected by earthquakes resulting from the permanent activities of the Cameroon volcanic line since the Cretaceous period. The results obtained in this work are crucial for future studies aimed at improving the exploitation of minerals and hydrocarbon resources and to update scientific knowledge on the structural geology of the region.

Funding

This research received no specific grant from funding agencies in the public, commercial, or not-for-profit sectors.

Competing interests statement

The authors have no competing interests to declare.

Author contributions

All authors contributed to the study's conception and design. Material preparation, data collection and analysis were performed by Paul Gautier Kamto, Erdinc Oksum and Luan Thanh Pham, Joseph Kamguia. The first draft of the manuscript was written by Paul

Gautier Kamto and Erdinc Oksum. All authors commented on previous versions of the manuscript. All authors read and approved the final manuscript.

Acknowledgments

The International Center for Global Gravity Field Models (ICGEM) is appreciated for providing the satellite gravity model XGM2019e free of charge on its web page. We thank the editor and reviewers for their comments on the manuscript. We are also grateful to the geodesy laboratory researchers of the National Institute of Cartography for their relevant observations to improve this work.

References

Amante C., Eakins B.W., 2009. ETOPO1 arcminute global relief model: procedures, data sources and analysis. NOAA technical memorandum NESDIS NGDC-24, National Geophysical Data Center, NOAA, 10.

Bournas N., Baker H.A., 2001. Interpretation of magnetic anomalies using the horizontal gradient analytic signal. Annals of Geophysics, 44, 505-526.

Brownfield M.E., Charpentier R.R., 2006. Geology and total petroleum systems of the West-Central Coastal Province (7203), West Africa. US Geological Survey, 2207-B, 52.

Cella F., Fedi M., Florio G., 2009. Toward a full multiscale approach to interpret potential fields. Geophysical Prospecting, 57(4), 543-557.

Chouhan A.K., 2020. Structural fabric over the seismically active Kachchh rift basin, India: insight from world gravity model 2012. Environmental Earth Sciences, 79(13), 1-14. https://doi:10.1007/s12665-020-09068-2.

Cooper G.R.J., Cowan D.R., 2006. Enhancing potential field data using filters based on the local phase. Computer & Geosciences, 32(10), 1585-1591.

Cordell L., Grauch V.J.S., 1985. Mapping basement magnetization zones from aeromagnetic data in the San Juan Basin. In: The utility of regional gravity and magnetic anomaly maps. Society of Exploration Geophysicists, 181-197.

Djomeni A.L., Ntamak-Nida M.J., Mvondo F.O., Kwetche P.G.F., Kissaaka J.B.I., Mooh-Enougui E., 2011. Soft-sediment deformation structures in Mid-Cretaceous to Mid-Tertiary deposits, Centre East of the Douala sub-basin, Cameroon: Preliminary results of the tectonic control. Syllabus Review, 2(3), 92-105.

Eldosouky A.M., Pham L.T., Duong V.H., Ghomsi F.E.K., Henaish A., 2022. Structural interpretation of potential field data using the enhancement techniques: a case study. Geocarto International, 37(27), 16900-16925.

Eldosouky A.M., Pham L.T., Mohammed H., Pradhan B., 2020. A comparative study of THG, AS, TA, Theta, TDX and LTHG techniques for improving source boundaries detection of magnetic data using synthetic models: a case study from G. Um Monqul, North Eastern Desert, Egypt. Journal of African Earth Sciences, 170. https://doi.org/10.1016/j.jafrearsci.2020.103940.

Elkhateeb S.O., Abdellatif M.A.G., 2018. Delineation potential gold mineralization zones in a part of Central Eastern Desert, Egypt using Airborne Magnetic and Radiometric data. NRIAG Journal of Astronomy and Geophysics, 7(2), 361-376.

Fedi M., Florio G., 2001. Detection of potential fields source boundaries by enhanced horizontal derivative method. Geophysical Prospecting, 49(1), 40-58.

Ferreira F.J.F., de Souza J., de Bongiolo A.B.eS., de Castro L.G., 2013. Enhancement of the total horizontal gradient of magnetic anomalies using the tilt angle. Geophysics, 78(3), 33-41.

Ghomsi F.E.K., Pham L.T., Tenzer R., Esteban F.D., Vu T.V., Kamguia J., 2022. Mapping of fracture zones and structural lineaments of the Gulf of Guinea passive margins using marine gravity data from CryoSat-2 and Jason-1 satellites. Geocarto International, 37(25), 10819-10842.

Hinze W.J., Frese R.R.B., Saad A.H., 2013. Gravity and magnetic exploration: principles, practices, and applications. New York: Cambridge University Press, 1-525.

Hsu S.K., Sibuet J.C., Shyu C.T., 1996. High- resolution detection of geologic boundaries from potential field anomalies: An enhanced analytic signal technique. Geophysics, 61(2), 373-1957.

Kamto P.G., Lemotio W., Tokam A.P.K., Yap L., 2021. Combination of terrestrial and satellite gravity data for the characterization of the southwestern coastal region of cameroon: appraisal for hydrocarbon exploration. International Journal of Geophysics, 1-14. https://doi.org/10.1155/2021/5554528.

Kenfack P.L., Njike P.R.N., Ekodeck G.E., Ngueutchoua, G., 2012. Fossils Dinoflagellates from the Northern Border of the Douala Sedimentary Sub-Basin (South-West Cameroon): Age Assessment and Paleoecological Interpretations. Geosciences, 2, 117-124.

Kumar S., Pal S.K., Guha A., Sahoo S.D., Mukherjee A., 2020. New insights on Kimberlite emplacement around the Bundelkhand Craton using integrated satellite-based remote sensing, gravity and magnetic data. Geocarto International, 1-23. https://doi:10.1080/10106049.2020.1756459.

Kwetche F.P., Ntamak N.M., Nitcheu A., Etame J., Mvondo F., Mbesse C., Kissaaka J., Ngon N.G., Bourquin S., Bilong P., 2018. Facies analysis and sequence stratigraphy of missole outcrops: N'Kapa Formation of the South-Eastern edge of douala sub-basin (Cameroon). Earth Science Research, Canadian Center of Science Education, 7, 35-54.

Lawrence S.R., Munday S., Bray R., 2002. Regional geology and geophysics of the eastern Gulf of Guinea (Niger Delta to Rio Muni). Lead Edge, 21(11), 1065-1176. https://doi.org/10.1190/1.1523752.

Ma G., Liu C., Li L., 2014. Balanced horizontal derivative of potential field data to recognize the edges and estimate location parameters of the source. Journal of Applied Geophysics, 108, 12-18.

Mbesse C.O., Roche E., Ngos III S., 2012. La limite Paleocene-Eocene dans le bassin de Douala (Cameroun), Biostratigraphie et essai de reconstruction des paléoenvironments par l'étude des Dinoflagellé. GeoEco-Trop, 36, 83-119.

Meyers J.B., Rosendahl B.R., Groschel-Becker H., Austin J.J.A., Rona P.A., 1996. Deep penetrating MCS imaging of the rift-to drift transition, offshore Douala and North Gabon basins, West Africa. Marine and Petroleum Geology, 13, 791-835. https://doi.org/10.1016/0264-8172(96)00030-X.

Mfayakouo B.C., Njike N.P.R., Bitom D.L., 2014. Sedimentary facies and depositional environments of Cenozoïc sedimentary Formations cropping out at the central part of the Douala basin. American Journal Geosciences, 4(1), 8-23. https://doi.org/10.3844/ajgs.2014.8.23.

Morley C.K., 1995. Developments in the structural geology of rifts over the last decade and their impact on hydrocarbon exploration. Geological Society, London, Special Publications, 80(1), 1-32.

Nasuti Y., Nasuti A., 2018. NTilt as an improved enhanced tilt derivative filter for edge detection of potential field anomalies. Geophysical Journal International, 214(1), 36-45.

Nasuti Y., Nasuti A., Moghadas D., 2019. STDR: A novel approach for enhancing and edge detection of potential field data. Pure and Applied Geophysics, 176(2), 827-841.

Nguene F.R., Tamfu S., Loule J.P., Ngassa C., 1992. Paléoenvironnements of the Douala and Kribi/Campo Subbasins in Cameroon, West African. Geologie Africaine : Colloque de Geologie Africaine, Libreville, Recueil des Communications, 6-8 May 1991, 129-139.

Oksum E., Dolmaz M.N., Pham L.T., 2019. Inverting gravity anomalies over the Burdur sedimentary basin, SW Turkey. Acta Geodaetica et Geophysica, 54, 445-460.

Oksum E., Le D.V., Vu M.D., Nguyen T.H.T., Pham L.T., 2021. A novel approach based on the fast sigmoid function for interpretation of potential field data. Bull. Geophys. Oceanogr, 62(3), 543-556.

Pal S.K., Vaish J., Kumar S., Priyam P., Bharti A.K., Kumar R., 2017. Downward continuation and Tilt Derivative of magnetic data for delineation of concealed coal fire in East Basuria Colliery, Jharia coal field, India. Journal of Earth System Science, 126(4), 1-17. https://doi.org/10.1007/s12040-017-0826-y.

Pauken R.J., Thompson J.M., Schuman J.R., Cooke J.C., 1991. Geology of the Douala Basin, offshore Cameroon. American Association of Petroleum Geologists Bulletin (United States), 75, 651-652.

Pham L.T., Do T.D., Oksum E., Le S.T., 2019. Estimation of Curie point depths in the Southern Vietnam continental shelf using magnetic data.

Vietnam J. Earth Sci., 41(3), 216-228. https://doi.org/10.15625/0866-7187/41/3/13830.

Pham L.T., Oksum E., Kafadar O., Trinh P.T., Nguyen D.V., Vo Q.T., Le S.T., Do T.D., 2022. Determination of subsurface lineaments in the Hoang Sa islands using enhanced methods of gravity total horizontal gradient. Vietnam J. Earth Sci., 44(3), 395-409. https://doi.org/10.15625/2615-9783/17013.

Pham L.T., Prasad K.N.D., 2023. Analysis of gravity data for extracting structural features of the northern region of the Central Indian Ridge. Vietnam J. Earth Sci.. https://doi.org/10.15625/2615-9783/18206.

Pham L.T., Le-Huy M., Oksum E., Do T.D., 2018. Determination of maximum tilt angle from analytic signal amplitude of magnetic data by the curvature-based method. Vietnam J. Earth Sci., 40(4), 354-366. https://doi.org/10.15625/0866-7187/40/4/13106.

Pham L.T., Oksum E., Le D.V., Ferreira F.J., Le S.T., 2021. Edge detection of potential field sources using the softsign function. Geocarto International, 37(14), 4255-4268.

Rao D.B., Prakash M.J., Ramesh B.N., 1990. 3-D and 2 1/2-D modeling of gravity anomalies with variable density contrast. Geophysical Prospecting, 38, 411-422.

Roest W.R.J., Verhoef J., Pilkington M., 1992. Magnetic interpretation using the 3-D analytic signal. Geophysics, 57(1), 116-125.

Tatchum N.C., Tabod C., Koumetio F., Manguelle-Dicoum E., 2011. A gravity model study for differentiating vertical and dipping geological contacts with application to a Bouguer gravity anomaly over the Foumban shear zone, Cameroon. Geophysica, 47, 43-55.

Ting-Jie Y.A.N., Yan-Gang W.U., Yuan Y.U.A.N., Ling-Na C.H.E.N., 2016. Edge detection of potential field data using an enhanced analytic signal tilt angle. Chinese Journal of Geophysics, 59(4), 341-349.

Van L.A.J., 2009. Soft-sediment deformation structures in siliciclastic sediments an overview. Geologos, 15(1), 3-55.

Wijns C., Perez C., Kowalczyk P., 2005. Theta map: edge detection in magnetic data. Geophysics, 70(4), 39-43.

Yuan Y., Yu Q., 2015. Edge detection in potential-field gradient tensor data by use of improved horizontal analytical signal methods. Pure and Applied Geophysics, 172(2), 461-472.

Zareie V., Moghadam R.H., 2019. The application of theta method to potential field gradient tensor data for edge detection of complex geological structures. Pure and Applied Geophysics, 176(11), 4983-5001.

Zhang X., Yu P., Tang R., Xiang Y., Zhao C.J., 2015. Edge enhancement of potential field data using an enhanced tilt angle. Exploration Geophysics, 46(3), 276-283.

Zingerle P., Pail R., Gruber T., Oikonomidou X., 2020. The combined global gravity field model XGM2019e. Journal of Geodesy, 94(7), 1-12.